Simulation of Human Benzo[a]pyrene Metabolism Deduced from the Analysis of Individual Kinetic Steps in Recombinant Yeast

ARTICLE *in* CHEMICAL RESEARCH IN TOXICOLOGY · APRIL 1996

Impact Factor: 3.53 · DOI: 10.1021/tx9500944 · Source: PubMed

4 AUTHORS, INCLUDING:

Jean-Charles Gautier
Sanofi Aventis Group
61 PUBLICATIONS **2,495** CITATIONS
SEE PROFILE

Philippe Urban
French National Centre for Scientific Research
50 PUBLICATIONS **1,899** CITATIONS
SEE PROFILE

Philippe Henri Beaune
Université René Descartes - Paris 5, AP-HP
390 PUBLICATIONS **15,845** CITATIONS
SEE PROFILE

Simulation of Human Benzo[*a*]pyrene Metabolism Deduced from the Analysis of Individual Kinetic Steps in Recombinant Yeast

Jean-Charles Gautier,[†] Philippe Urban,[‡] Philippe Beaune,*[,†] and Denis Pompon[‡]

INSERM U75, CHU Necker-Enfants-Malades, Université René Descartes, 75015 Paris, France, and Centre de Génétique Moléculaire du CNRS, Laboratoire Propre associé à l'Université Pierre et Marie Curie, 91198 Gif-sur-Yvette, Cedex France

Received May 31, 1995[⊗]

Human cytochrome P450 1A1 (1A1) and microsomal epoxide hydrolase (mEH)-dependent metabolic activation of benzo[*a*]pyrene (BP) have been reconstituted with microsomes from yeast cells expressing the two enzymes. The formation of the postulated ultimate mutagen 7*β*,8α-dihydroxy-9α,10α-epoxy-7,8,9,10-tetrahydro-BP, the so-called diol epoxide-2 (DE2) derived from the reoxidation of BP-7,8-dihydrodiol by 1A1, was estimated by HPLC measurement of its hydrolysis product 7*β*,8α,9α,10*β*-tetrahydrotetrol-BP (T2-tetrol). The 1A1/mEH coupled system was analyzed by varying the incubation time, initial substrate concentration, and molar ratio of the two enzymes. A minimum kinetic model of BP metabolism by 1A1 and mEH was constructed on the basis of the overall kinetic parameters (V_{max}, K_m) for a number of individual steps determined with human 1A1 and mEH expressed in yeast. The model was converted into a set of differential equations including 30 independent kinetic constants, 15 chemical species, and 8 enzymes and enzyme/substrate complexes. Numerical simulation of the model enabled us to satisfactorily reproduce the experimental kinetics of formation of BP-phenols, -dihydrodiols, and -tetrols for all tested conditions. Such a validated model was used to investigate the kinetics of unstable genotoxic species such as BP-epoxides and diol epoxides, which were not directly measurable. Based on numerical simulation, BP-7,8-oxide and -9,10-oxide appear to accumulate rapidly to reach a plateau after 2 min, while maximal accumulation of DE2 occurs after about a half-hour and declines during the following 2 h. A contribution of BP-9,10-dihydrodiol metabolism to T2-tetrol formation via the formation of a BP-7,8-oxide-9,10-dihydrodiol is predicted to be detectable after 2 hours due to the preferential accumulation of BP-9,10-dihydrodiol following 1A1-dependent consumption of initially accumulated BP-7,8-dihydrodiol.

Benzo[*a*]pyrene (BP),[1] a polycyclic aromatic hydrocarbon, is a widespread environmental pollutant found in incomplete combustion products. This compound was described as a possible causative agent of lung cancer in smokers (*1*, *2*). It has been shown that BP can be oxidized by human cytochrome P450 1A1 (1A1) into BP-7,8-epoxide (7,8-ox), which is hydrolyzed by microsomal epoxide hydrolase (mEH) into BP-7,8-dihydrodiol (7,8-diol). The latter compound can then be reoxidized by 1A1 to give the postulated ultimate mutagen 7*β*,8α-dihydroxy-9α,10α-epoxy-7,8,9,10-tetrahydro-BP, the so-called diol epoxide-2 (DE2) (*3*). Either this diol epoxide can be spontaneously hydrolyzed into tetrols, or it reacts with DNA to form adducts. Alternatively, BP can be oxidized by 1A1 on other positions of the molecule to produce epoxides which can be either spontaneously rearranged into phenols such as 3-hydroxy-BP (3-OH) and 9-OH, or enzymatically hydrolyzed by mEH into dihydrodiols such as 4,5-diol and 9,10-diol. Although the metabolism of BP has been investigated with human 1A1 and mEH expressed in several expression systems (*4*−*7*), the kinetics of DE2 formation from BP has not been studied.

Knowledge of the time course for unstable species is of critical importance when genotoxic events are associated. In particular, this opens up the possibility of analysis of the potential role of the dynamics of genotoxic damage in modulating the mutagenesis/repair balance. In the case of BP, accumulation of reactive species could be critically determined by the ratio between 1A1 and mEH, and by the rate of nonenzymatic processes such as spontaneous rearrangement, chemical hydrolysis, and adduct formation. In addition, competition between BP and derivatives at the 1A1 and mEH active sites could result in rather unpredictable behavior in the absence of detailed knowledge of individual reaction rates and substrate affinities. The qualitative description of the BP metabolite pattern is thus not sufficient for predicting the consequences of polymorphisms which could affect both enzymatic kinetic parameters and relative expression levels.

The first two steps of BP activation leading to the formation of 7,8-diol have been previously reconstituted by coexpression of human 1A1 and mEH in the yeast *Saccharomyces cerevisiae* (*7*). Efficient metabolic coupling was observed even when the two enzymes were included in separate microsomal membranes. We now report a complementary investigation using an optimized HPLC detection system permitting simultaneous quan-

* Author to whom correspondence should be addressed.
† INSERM U75. FAX: 33 1 40 61 55 82; e-mail: pbeaune@citi2.fr.
‡ CNRS. FAX: 33 1 69 07 55 39; e-mail: pompon@cgm.cnrs-gif.fr.
⊗ Abstract published in *Advance ACS Abstracts,* February 1, 1996.
[1] Abbreviations: BP, benzo[*a*]pyrene; 7,8-ox, BP-7,8-oxide; 3-OH, 3-hydroxy-BP; 7,8-diol, BP-7,8-dihydrodiol (other BP-oxides, BP-phenols, and BP-dihydrodiols are similarly abbreviated); DE2, diol epoxide-2; DE3, diol epoxide-3; T2-tetrol, 7*β*,8α,9α,10*β*-tetrahydrotetrol; C2-tetrol, 7*β*,8α,9α,10α-tetrahydrotetrol; P450, cytochrome P450; mEH; microsomal epoxide hydrolase; 1A1, cytochrome P450 1A1.

0893-228x/96/2709-0418$12.00/0

titation of a large number of metabolites (phenols, dihydrodiols, and also tetrols derived from spontaneous hydrolysis of diol epoxides). The results obtained with the yeast-expressed human enzymes were used to establish a minimal kinetic model for BP multistep metabolism. The present study confirms that numerical simulation of the presented model can satisfactorily reproduce experimental kinetics, and thereafter can be used to predict the concentration courses for highly unstable epoxides and diol epoxides which cannot be quantified directly.

Materials and Methods

Chemicals and Reagents. Caution: *BP and its derivatives are probable human carcinogens. They should be handled in accordance with NIH guidelines* (*8*).

BP, benzo[*ghi*]perylene, NADP(H), and trifluoroacetic acid were purchased from Sigma (St. Louis, MO, USA). [^{3}H]BP (specific activity 80 Ci/mmol) was from Amersham (Les Ulis, France). Racemic 3-OH, 9-OH, and *trans*-7,8-diol were obtained from the National Cancer Institute Chemical Repository (Midwest Research Institute, Kansas City, MO, USA). Racemic *trans*-4,5-diol and *trans*-9,10-diol were kindly donated by Dr. P. Dansette. Racemic 7β,8α,9α,10β-tetrahydrotetrol (T2-tetrol) and 7β,8α,9α,10α-tetrahydrotetrol (C2-tetrol) were a kind gift from Dr. F. Oesch and Dr. A. Seidel. Octyldecylsilyl Newguards (7 μm particle size, 15 mm × 3.2 mm) and Spheri-5 columns (5 μm particle size, 100 mm × 2.1 mm) were from Brownlee (San Jose, CA, USA).

Yeast Strains, Culture, and Microsome Preparation. Yeast strains W[R]-pV60, W[R]-p1A1, W[R]-pEH, and W[E,R]-p1A1 have been described previously (*7*). Briefly, all these strains were genetically engineered to overexpress yeast NADP-(H) cytochrome P450 reductase when grown in the presence of galactose. W[R]-pV60 corresponds to the control strain transformed with cDNA-free pV60. W[R]-p1A1 and W[R]-pEH express respectively human 1A1 and mEH. W[E,R]-p1A1 coexpresses human 1A1 and mEH. All strains were grown in minimum galactose medium SW5 until cell density reached A_{600} of 3 (*9*) and diluted 3-fold with complete medium YPL containing galactose, and cell growth was continued up to A600 of 10. Microsomes were prepared using an enzymatic lysis method (*10*). Total P450 content was calculated from the reduced carbon monoxide difference spectra (*11*) using a Perkin-Elmer Lambda 2 spectrophotometer. The concentration of mEH was evaluated by measuring the styrene oxide hydrolase activity as described (*7*). Protein concentration was determined using the Pierce bicinchoninic acid procedure, according to the manufacturer's instructions.

Reverse Phase HPLC of BP Metabolites. BP (0−15 μM) was incubated for 15 min at 37 °C in 50 mM Tris-HCl buffer, pH 7.4, 1 mM EDTA, 0.1 mg/mL NADP(H), and 150 μg of microsomal proteins in a final volume of 200 μL. All experiments were performed using the same membrane to buffer volume ratio to limit possible artifacts resulting from partition effects of BP between membrane and aqueous phases. Adjustment of membrane to buffer ratio was achieved when required by addition of control yeast microsomes (from strain W[R]-pV60) devoid of 1A1 and mEH. Reactions were generally stopped with 16 μL of trifluoroacetic acid 25% in water in order to secure hydrolysis of oxides. A drawback of this procedure is the almost stoichiometric conversion of the 9,10-diol to 9-OH. Trifluoroacetic acid was thus omitted when measuring the formation of 9,10-diol. We checked that the latter procedure did not affect the formation of T2-tetrol in our experimental conditions. Extractions were performed using 200 μL of ethyl acetate and 200 μL of NaCl-saturated water. Benzo[*ghi*]perylene (1.2 nmol) was added as an internal standard. Organic extracts were evaporated under a nitrogen stream, and residues were solubilized in 80 μL of methanol 50% in water. A 10-μL aliquot was analyzed by HPLC. Metabolite separations were accomplished on a 100-mm octyldecylsilyl column (Brownlee). Elution was carried out at a flow rate of 1 mL/min, using a rapid gradient just after the injection start from 0% to 15% acetonitrile in water (containing 0.02% trifluoroacetic acid), followed successively by a linear gradient of 15−40% acetonitrile for 16 min, a 6-min gradient to 50% acetonitrile, a 9-min gradient to 75% acetonitrile, and finally a rapid gradient to pure acetonitrile. We checked that 9,10-diol was not converted into 9-OH in our HPLC conditions. The column effluent was monitored by using a Jasco 821 FP fluorescence detector, set with the following program: λ_{exc} = 340 nm, λ_{em} = 402 nm from 0 to 12 min (for tetrols); λ_{exc} = 278 nm, λ_{em} = 407 nm from 12 to 14 min (for 9,10-diol); λ_{exc} = 263 nm, λ_{em} = 388 nm from 14 to 16 min (for 4,5-diol); λ_{exc} = 348 nm, λ_{em} = 402 nm from 16 to 19 min (for 7,8-diol); λ_{exc} = 375 nm, λ_{em} = 435 nm from 19 to 40 min (for 9-OH, 3-OH, BP, and benzo[*ghi*]perylene). The BP metabolite concentrations were deduced from the peak areas on the chromatograms using authentic compounds for calibration. Incubations with labeled BP were performed as described above, except that 25 μCi of [^{3}H]BP was added. BP-quinones were quantified by scintillation counting after HPLC fraction collection from 18 to 21 min using a Gilson 201 collector. Enzymatically synthesized 7,8- and 9,-10-diols were purified by preparative HPLC using a Gilson 201 collector and were subsequently used as substrate for 1A1, as described for BP.

Numerical Simulation. The kinetic model of BP metabolism by 1A1 and mEH presented in Figure 3 was converted into a set of differential equations listed in Table 2. Numerical integration was used to solve the set of differential equations for the given initial concentrations of reagents (see legends of Figures 4−7 for BP, 1A1, and mEH concentrations) and the given rate constants (Table 3). An interactive home made simulation program for a Macintosh microcomputer was used to calculate all the presented data. This integration program was written and compiled using Symantech Think Pascal object-oriented language and Water's Edge Software ToolsPlus interface libraries. Integration was based on a fourth order Runge-Kuta method (*12*) with an automatic step control, interactive graphic interface, and batch mode capability. The program can be made available as a standard self-sufficient Macintosh application associated with predefined rate constants and initial concentration files. From a practical point of view, 4 cases of increasing complexity can be considered:

Case 1: The model is used as such with the given rate constants and the given initial concentrations of chemicals and enzymes. The program, once launched, allows the reader to recalculate the time course of all species in the model.

Case 2: The model is used as such, but with different rate constants and/or different enzyme or chemical concentrations. This case is similar to Case 1, except that rate constant files and concentration files must be rebuilt. The self-sufficient application stated in Case 1 enables rebuilding through a standard Macintosh dialogue in various windows. This gives readers the possibility of testing the influence of relative rate constants and concentrations on species kinetics.

Case 3: The model also has to be changed (a different model, species, new reactions, and new constants), but the total numbers of constants and species are not significantly increased. The differential equation set has to be rebuilt accordingly and introduced using the "Pascal" language syntax into the "model" module of the source code (written Pascal). The new module must be compiled and linked to the main simulation program, which requires a commercial program, *i.e.*, "Think Pascal" from Symantech (and the corresponding license) or, for the forthcoming version of the simulation program, the CW6 version of the CodeWarrior C++ and Pascal Macintosh development package.

Case 4: Extensive changes in the model are required, including much more complex models. Full knowledge of the program and total source code (several thousand lines) is required. Please contact the author, Denis Pompon.

Table 1. Metabolism of BP by Human 1A1 and mEH Expressed in Yeast[a]

microsomes	BP metabolite formation rate (pmol·(pmol of P450)$^{-1}$·min^{-1})					
	T2-tetrol	9,10-diol	4,5-diol	7,8-diol	9-OH	3-OH
1A1[b]	<0.01	<0.01	0.07 ± 0.05	<0.01	3.32 ± 0.87	5.82 ± 1.43
1A1+ mEH[c] (mixtures)	0.10 ± 0.01	0.89 ± 0.20	0.23 ± 0.04	2.55 ± 0.58	1.98 ± 0.39	5.36 ± 0.84
1A1+ mEH[d] (coexpression)	0.14 ± 0.07	1.22 ± 0.13	0.14 ± 0.07	2.06 ± 0.47	2.03 ± 0.12	4.86 ± 1.71

[a] BP (15 μM) was incubated for 15 min at 37 °C in 50 mM Tris-HCl buffer, pH 7.4, in the presence of yeast microsomes and arrested without trifluoroacetic acid. Turnover numbers were calculated based on the 1A1 concentration determined by spectral titration. Values are the average ± SD of 5 determinations. [b] Microsomes from strain W[R]-p1A1 (1A1 = 5 nM). [c] Mixture of microsomes from strain W[R]-p1A1 (1A1 = 5 nM) and microsomes from strain W[R]-pEH (mEH = 20 nM). [d] Microsomes from strain W[E,R]-p1A1 (1A1 = 5 nM, mEH = 20 nM).

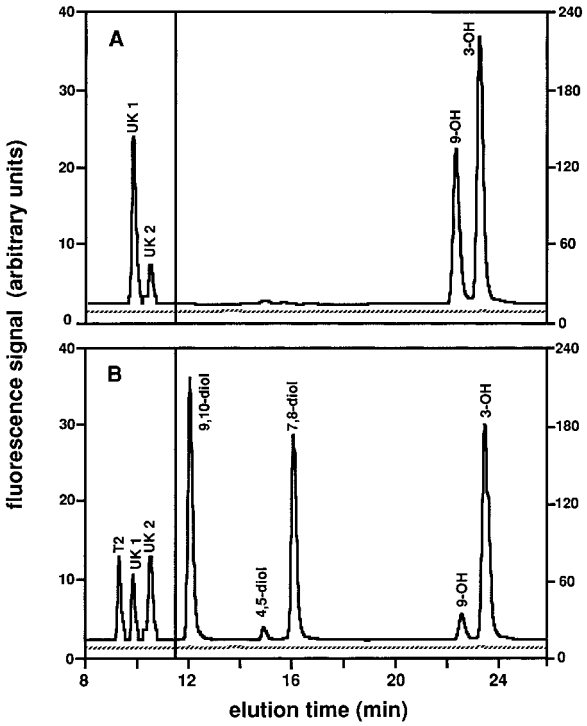

Figure 1. HPLC profiles upon incubation of BP with (A) yeast microsomes from strain W[R]-p1A1 containing 5 nM of human 1A1 (—), control microsomes from strain W[R]-pV60 (- - -); (B) a mixture of microsomes from strain W[R]-p1A1 containing 5 nM human 1A1 and from strain W[R]-pEH containing 100 nM mEH (—), a mixture of control microsomes from strain W[R]-pV60 and from strain W[R]-pEH containing 100 nM mEH (- - -). Reactions were stopped with ethyl acetate in order to visualize 9,10-diol. The fluorescence scale for the left-hand side of the figure (tetrol zone) is enlarged 6-fold as compared to the right-hand side. UK1, UK2: unknown metabolites.

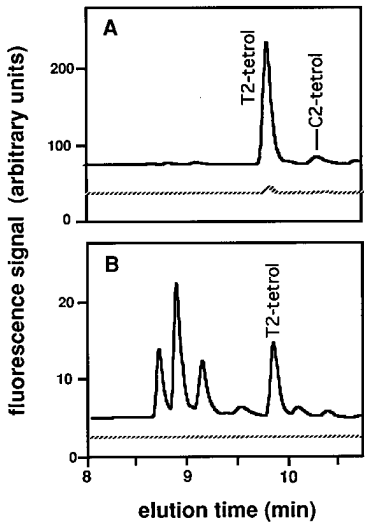

Figure 2. HPLC profiles upon incubation of (A) enzymatically synthesized 7,8-diol with yeast microsomes from strain W[R]-p1A1 containing 5 nM of 1A1 (—), control microsomes from strain W[R]-pV60 (- - -); (B) enzymatically synthesized 9,10-diol with microsomes from strain W[R]-p1A1 containing 5 nM of 1A1 (—), control microsomes from strain W[R]-pV60 (- - -). Reactions were stopped with trifluoroacetic acid. Fluorimetric scale of traces from incubations with 9,10-diol was enlarged 10-fold compared to traces from incubations with 7,8-diol. Peaks to the left of T2-tetrol in traces from incubations with 9,10-diol correspond to unidentified polar metabolites.

Results and Discussion

Steady State Parameters for BP Metabolism by Human 1A1 and mEH Expressed in Yeast. BP was incubated with 1A1-containing yeast microsomes mixed or not mixed with mEH-containing yeast microsomes. The HPLC metabolite profile shown in Figure 1A indicates that essentially 3-OH and 9-OH were produced with 1A1 alone. By contrast, addition of mEH dramatically enhanced the rate of formation of 9,10-diol, 7,8-diol, and 7β,8α,9α,10β-tetrahydrotetrol (T2-tetrol), which is the major hydrolysis product of the postulated ultimate mutagen DE2 (*13*) (Figure 1B). A concomitant decrease in 9-OH, a spontaneous rearrangement product of 9,10-ox, is consistent with mEH-dependent hydrolysis of the oxide to the corresponding dihydrodiol. BP-quinones which escape fluorescence detection were found to represent about 15% of the total [^{3}H]-labeled metabolites formed, independently of the presence of mEH; they will be considered as a whole in the kinetic model described below. Apparent turnover numbers relative to 1A1 for the formation of phenols, dihydrodiols, and T2-tetrol from BP appeared identical (within experimental variation) when mixtures of microsomes were compared with microsomes from a coexpression system in which human 1A1 and mEH were located in the same membranes (Table 1). This indicates that diffusion steps of BP-oxides and -dihydrodiols between microsomal membranes are not a limiting factor, confirming previously published results (*7*).

In order to determine the kinetic parameters of each BP metabolic step, the 7,8- and 9,10-diols enzymatically synthesized by human 1A1 and mEH combined actions were recovered from preparative HPLC. Incubation of the purified 7,8-diol with 1A1 resulted in the formation of T2- and C2-tetrols, the hydrolysis products of DE2 (Figure 2A). Incubation of 1A1 with enzymatically synthesized 9,10-diol (Figure 2B) also led to the formation of T2-tetrol, indicating that a BP-7,8-oxide-9,10-dihydrodiol intermediate, called diol epoxide-3 (DE3) in the present paper, was produced. The apparent turnover number of 1A1 for the formation of T2-tetrol from 9,10-diol was determined and found to be lower (3 min^{-1}) than for the formation of T2-tetrol from 7,8-diol (30 min^{-1}). Nevertheless, in the case of the 9,10-diol incubation, additional formation of unidentified metabolites, more

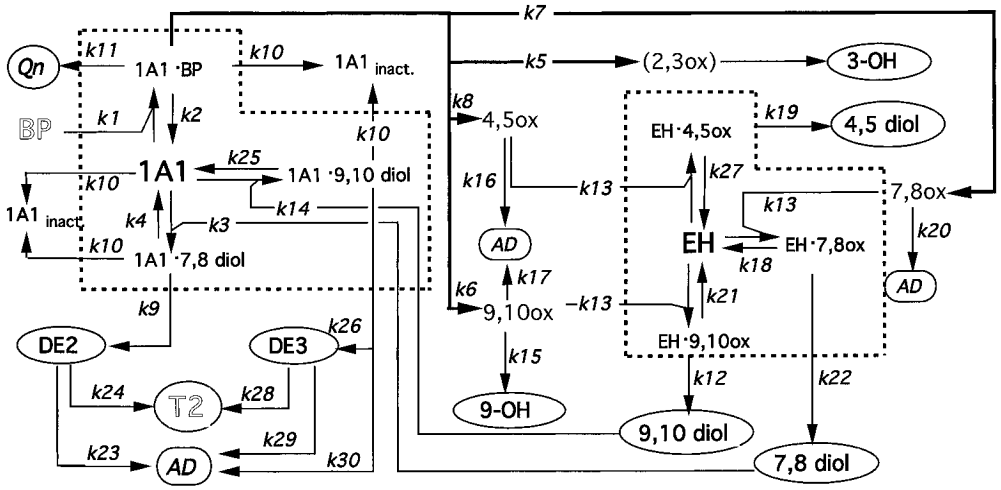

Figure 3. Kinetic model for BP metabolism. 1A1 and mEH complexes are indicated as boxed areas with dotted lines on the left and right part of the figure, respectively. The indexes of kinetic constants are defined close to arrows. Abbreviations: $1A1_{inact.}$: inactivated 1A1; AD: covalent adducts or unidentified products; T2: T2-tetrol; Qn: quinones; 1A1·metabolite: complexes between 1A1 and substrate; EH·metabolite: complexes between mEH and substrate.

polar than tetrols, was observed (their overall formation rate was estimated to be 15 min^{-1}, assuming a similar response factor as tetrols for the fluorescence signal measured by HPLC). Based on accumulation of T2-tetrol, the formation of DE2 from 7,8-diol and of DE3 from 9,-10-diol behaved as saturable enzymatic processes with apparent K_m of about 0.7 μM and 15 μM, respectively. In addition, comparison of 7,8-diol consumption with the sum of T2- and C2-tetrol formation suggested that production of other compounds (putatively diol epoxide adducts) took place and represented twice the amount of observed tetrols. No detectable metabolite formation was observed upon incubation of 1A1 with chemically synthesized 3-OH, 9-OH, and 4,5-diol.

Minimal Kinetic Model for the Multistep Metabolism of BP. A basic kinetic model of BP metabolism by 1A1 and mEH was established on the basis of previous experiments performed with yeast-expressed human enzymes. Figure 3 illustrates that competition between BP, 7,8-diol and 9,10-diol at the 1A1 active site level was represented by assuming a single binding site. Possible inhibition by other metabolites (3-OH, 9-OH, 4,5-diol, and T2-tetrol) was not considered. Similarly, competition between the three BP-oxides (4,5-ox, 7,8-ox, 9,10-ox) at the mEH active site level was represented supposing a single binding site. The 2,3-ox was not considered, as it converted spontaneously at a high rate into 3-OH (*14*) and thus should not accumulate even in the absence of mEH. In the case of 9,10-ox, two reactions were considered: spontaneous isomerization to 9-OH and mEH-dependent hydrolysis to 9,10-diol. For the three BP-oxides, conversion to unidentified or undetected compounds, for example, 7-OH from 7,8-ox (*15*), or adduct formation, was represented by an overall reaction step leading to the generic adduct formation. T2-tetrol formation arose from the hydrolysis of either DE2 or DE3. No enzymatic hydrolysis step of DE2 and DE3 was included, so as to remain consistent with the absence of apparent hydrolysis by mEH. As in the case of simple BP-oxides, formation of adducts and unidentified compounds from DE2 and DE3 was represented by a common reaction step leading to generic adduct formation.

Adjustment of Kinetic Constants. The kinetic model illustrated in Figure 3 was converted into a set of differential equations listed in Table 2 in order to perform numerical simulations (see Materials and Methods). Values for the 1A1 concentrations used in the model were recalculated based on the experimental rate of 3-OH formation and on the determined average turnover number (Table 1), since it represents the actual active 1A1. Concentrations of mEH were evaluated from styrene oxide hydrolase activity measured on microsome preparations using the published turnover number (*16*).

The kinetic constants used in the model are listed in Table 3. The ratio k_2/k_1 of dissociation and association constants between BP and 1A1 was adjusted based on the apparent K_m for 3-OH formation. Although this ratio was correctly determined, absolute values for k_1 and k_2 could not be accessed and were chosen in order to be nonlimiting. Dissociation (k_4) and association (k_3) constants for 7,8-diol binding to 1A1 were initially determined from the experimental K_m and subsequently corrected by trial and error adjustments of the rate and shape of T2-tetrol formation versus time, BP concentration, and mEH to 1A1 ratio. Constants k_{25} and k_{14} for 9,10-diol binding to 1A1 were estimated on the basis of the corresponding K_m. Rate constants k_5, k_6, k_7, and k_8, for the formation of 3-OH, 9,10-ox, 7,8-ox, and 4,5-ox, respectively, were deduced by trial and error adjustments based on the experimental kinetic courses of 3-OH, 9-OH, 9,10-diol, 7,8-diol, and 4,5-diol. An inactivation step for 1A1 (k_{10}) was introduced to account for the observed inactivation during incubations. The constant k_{10} was adjusted based on the time course of total observable metabolites. The dissociation and association constants between 7,8-ox and mEH were based on a K_m for 7,8-ox in the range of 1 μM (*17*). The same values were assumed for 9,10-ox and 4,5-ox binding constants. The ratios between the rate constants for mEH-dependent hydrolysis of oxides (k_{19}, k_{22}, k_{12}) and for chemical rearrangements of oxides (k_{16}, k_{20}, k_{15}, k_{17}) were determined from simulation of the metabolite profiles as a function of mEH concentration. Half-lives for BP-oxides were taken from literature data (*18*). Constants k_{23}, k_{24}, k_{28}, and k_{29} of adducts and T2-tetrol formation from DE2 and DE3 were evaluated based on the total rate of dihydrodiol consumption upon incubation with 1A1. Absolute hydrolysis rate constants for DE2 and DE3 were chosen so as to be nonlimiting.

Table 2. Differential Equations for Numerical Simulation of the Model[a]

species X	d[X]/d*t*
BP	k_2[1A1·BP] + k_{10}[1A1·BP] − k_1[BP][1A1]
1A1	k_4[1A1·7,8-diol] + (k_{25} + k_{30} + k_{26})[1A1·9,10-diol] + k_9[1A1·7,8-diol] + k_{11}[1A1·BP]+ k_2[1A1·BP]+ (k_5 + k_6 + k_7 + k_8)[1A1·BP] − k_1[1A1][BP] − k_{14}[1A1][9,10-diol] − k_{10}[1A1] − k_3[1A1][7,8-diol]
$1A1_{inactiv.}$	k_{10}([1A1] + [1A1·7,8-diol] + [1A1·BP] + [1A1·9,10-diol])
1A1·BP[b]	k_1[BP][1A1] − (k_5 + k_6 + k_7 + k_8 + k_2 + k_{10} + k_{11})[1A1·BP]
4,5-ox	k_8[1A1·BP] + k_{27}[EH·4,5-ox] − k_{16}[4,5-ox] − k_{13}[EH][4,5-ox]
7,8-ox	k_7[1A1·BP] + k_{18}[EH·7,8-ox] − k_{20}[7,8-ox] − k_{13}[EH][7,8-ox]
9,10-ox	k_6[1A1·BP] + k_{21}[EH·9,10-ox] − k_{13}[EH][9,10-ox] − k_{17}[9,10-ox] − k_{15}[9,10-ox]
3-OH	k_5[1A1·BP]
9-OH	k_{15}[9,10-ox]
quinones	k_{11}[1A1·BP]
EH	(k_{12} + k_{21})[EH·9,10-ox] + (k_{18} + k_{22})[EH·7,8-ox] + (k_{27}+ k_{19})[EH·4,5-ox] − k_{13}[EH] ([4,5-ox] + [7,8-ox] + [9,10-ox])
EH·4,5-ox[b]	k_{13}[4,5-ox][EH] − (k_{27} + k_{19})[EH·4,5-ox]
EH·7,8-ox[b]	k_{13}[7,8-ox][EH] − (k_{18} + k_{22})[EH·7,8-ox]
EH·9,10-ox[b]	k_{13}[9,10-ox][EH] − (k_{21} + k_{12})[EH·9,10-ox]
4,5-diol	k_{19}[EH·4,5-ox]
7,8-diol	k_{22}[EH·7,8-ox] + k_4[1A1·7,8-diol] + k_{10}[1A1·7,8-diol] − k_3[1A1][7,8-diol]
9,10-diol	k_{12}[EH·9,10-ox] + k_{25}[1A1·9,10-diol] + k_{10}[1A1·9,10-diol] − k_{14}[9,10-diol][1A1]
1A1·7,8-diol[b]	k_3[1A1][7,8-diol] − (k_4 + k_9 + k_{10})[1A1·7,8-diol]
1A1·9,10-diol[b]	k_{14}[1A1][9,10-diol] − (k_{25} + k_{10} + k_{26} + k_{30})[1A1·9,10-diol]
DE2	k_9[1A1·7,8-diol] − (k_{23} + k_{24})[DE2]
DE3	k_{26}[1A1·9,10-diol] − (k_{29} + k_{28})[DE3]
T2-tetrol	k_{24}[DE2] + k_{28}[DE3]
adducts	k_{17}[9,10-ox] + k_{20}[7,8-ox] + k_{16}[4,5-ox] + k_{23}[DE2] + k_{29}[DE3] + k_{30}[1A1·9,10-diol]

[a] Reactions correspond to those shown in Figure 3. [b] Enzyme/substrate complexes.

Table 3. Kinetic Constants for the Model[a]

enzyme/substrate complexes	association constants[b] ($\mu M^{-1}\cdot min^{-1}$)	dissociation constants[b] (min^{-1})	products	catalytic constants[c] (min^{-1})	products	nonenzymatic constants[d] (min^{-1})
1A1·BP	k_1 = 30	k_2 = 100				
			2,3-ox	k_5 = 14		
			4,5-ox	k_8 = 0.7	adducts	k_{16} = 0.004
			7,8-ox	k_7 = 10	adducts	k_{20} = 0.018
			9,10-ox	k_6 = 10	adducts	k_{17} =0.1
					9-OH	k_{15} = 0.3
			quinones	k_{11}= 5.2		
1A1·7,8-diol	k_3 = 40	k_4 = 100				
			DE2	k_9 = 85	adducts	k_{23} = 60
					T2-tetrol	k_{24} = 30
1A1·9,10-diol	k_{14} = 26	k_{25} = 100				
			DE3	k_{26} = 4.5	adducts	k_{29} = 40
					T2-tetrol	k_{28} = 60
			adducts	k_{30} = 15		
mEH·4,5-ox	k_{13} = 180	k_{27} = 100				
			4,5-diol	k_{19} = 23		
mEH·7,8 ox	k_{13} = 180	k_{18} = 100				
			7,8 diol	k_{22} = 11.5		
mEH·9,10 ox	k_{13} = 180	k_{21} = 100				
			9,10 diol	k_{12} = 7.5		

[a] Values of rate constants are complementary data required to perform calculations with the set of differential equations listed in Table 2. Inactivation of 1A1 was simulated as a first-order inactivation reaction (k_{10} = 0.022 min^{-1}) in the experimental conditions of buffer and temperature used. [b] Association/dissociation constants are, respectively, second- and first-order rate constants relative to the formation/dissociation of the indicated complexes (first column). [c] Catalytic constants are the first-order rate constants for formation of the indicated products (fourth column). [d] Nonenzymatic constants are first-order rate constants for spontaneous conversions giving the stated products (sixth column).

Comparison between Experimental and Simulated Kinetics. (a) Time Dependence of BP Metabolite Formation. The experimental time course of BP metabolite accumulation using the mix strategy is illustrated in Figure 4, left panel. Formation of 3-OH, which required only a single enzymatic step, was relatively linear versus time. Nevertheless, some decreases in the rate of metabolite formation could be detected for an incubation time longer than 10 min. Experimental kinetics of T2-tetrol accumulation presented a reproducible lag time of about 2 min. In contrast, no detectable lag was observed for dihydrodiol formation. This suggests that the delay in tetrol accumulation was related to recapture of 7,8-diol by 1A1. Very similar results were obtained using microsomes from the coexpression system (data not shown).

Accurate simulation was achieved with the kinetic model described previously, particularly for the T2-tetrol lag time (Figure 4, right panel and left panels were superimposable). The 1A1 inactivation constant k_{10} was adjusted to 0.022 min^{-1} to fit experimental data up to 30 min. Inclusion of diffusion steps between microsomes containing, respectively, 1A1 and mEH was not required to simulate data obtained with microsome mixes. To further test this finding, the model presented was modified by adding intermembrane diffusion steps of epoxides and dihydrodiols. First order diffusion constants between membranes lower than 1 min^{-1} caused a simulated lag time for dihydrodiol formation (not shown) incompatible with experimental data. In contrast, a higher rate of diffusion (5 min^{-1}) led to almost identical simulations with and without the diffusion steps. We thus concluded

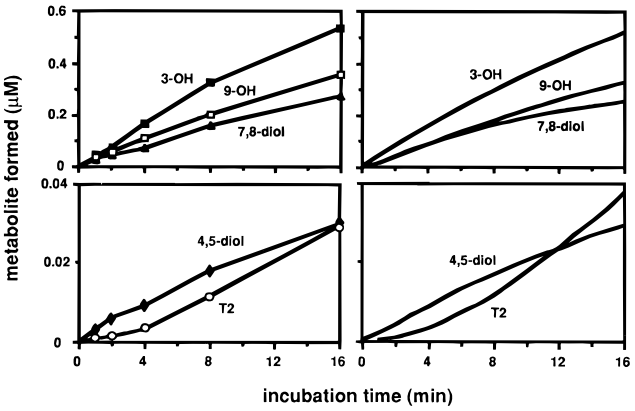

Figure 4. Time dependence of BP metabolite accumulation after incubation with microsome mixes (from strains W[R]-p1A1 and W[R]-pEH) containing 5.8 nM 1A1 and 100 nM mEH. Initial BP concentration was 5 μM. Reactions were stopped by addition of trifluoroacetic acid. Left panel: experimental traces; right panel: simulated traces according to the set of differential equations listed in Table 2, rate constants indicated in Table 3, and experimental enzyme and BP concentrations. The 9-OH trace corresponds to the sum of spontaneously formed 9-OH and acid-converted 9,10-diol.

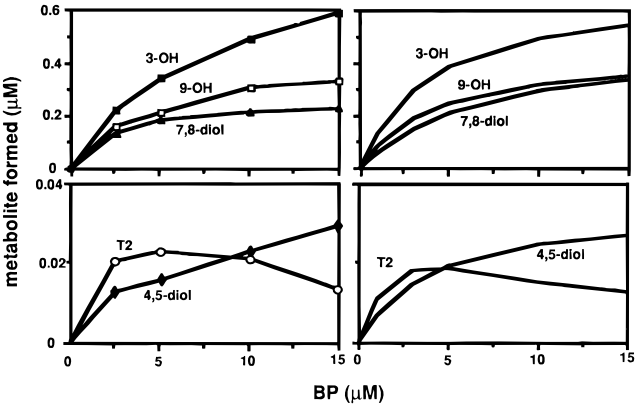

Figure 5. Dependence of the metabolite profile on initial BP concentration after incubation (15 min at 37 °C) with a mix of microsomes (from strains W[R]-p1A1 and W[R]-pEH) containing 3.8 nM 1A1 and 100 nM mEH. Reactions were stopped by trifluoroacetic acid, causing complete conversion of 9,10-diol to 9-OH. Left panel: experimental traces; right panel: simulated traces using the same equations and constants used in Figure 4, and the actual 1A1 and mEH experimental concentrations. To take into account the experimental conversion of 9,10-diol to 9-OH, these two concentrations were added up in the simulation.

that, in the experimental conditions used, diffusion between membranes was not limiting. This finding is in agreement with the reported analysis of the kinetics of BP diffusion between phospholipid micelles (*19*). The microsome "mix" strategy is very convenient and could thus be valid even when short-lived intermediates are involved.

(b) Course of Metabolite Formation versus BP Concentration. The experimental kinetics of T2-tetrol accumulation versus BP concentration present a bell-shaped aspect with a maximum in the range of 2−4 μM (Figure 5, left panel). Thus, inhibition of 1A1-dependent dihydrodiol oxidation by BP limits the formation of genotoxic species. Very similar results were obtained using microsomes from the coexpression system (data not shown).

The simulated kinetics showed very good fit with experimental kinetics when using the same set of constants as used for time kinetic simulation (Figure 5, compare right panel to left panel). Parameters for the dissociation and association of 7,8-diol to 1A1 (k_3, k_4) were initially chosen on the basis of saturation data obtained by using 7,8-diol as the sole substrate (K_m = 0.7 μM). Nevertheless, this choice led to a simulated rate of T2-tetrol formation from BP which was much higher than experimentally observed. Improved simulation of experimental data required a 6-fold decrease in the value of the association constant k_3. This prompted us to reinvestigate experimental saturation by 7,8-diol in the presence of variable amounts of BP. Half-inhibition of 7,8-diol oxidation was observed in the presence of an equal concentration of BP (1 μM). This result is simply interpreted as resulting from a similar apparent affinity of BP and 7,8-diol for the 1A1 active site. Comparison of this inhibition experiment with half-saturation concentrations for BP (4 μM) and 7,8-diol (0.7 μM), when tested separately, suggested a nonclassical mechanism of inhibition of 7,8-diol metabolism by BP.

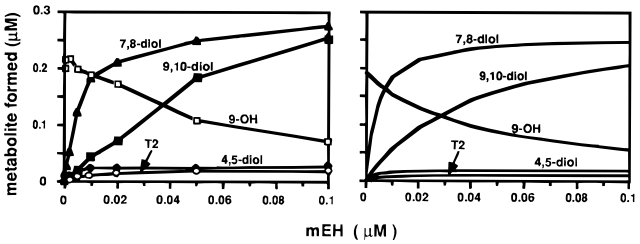

Figure 6. Influence of the ratio of mEH to 1A1 concentrations on BP metabolite formation. Incubations were performed with a constant 1A1 concentration (3.8 nM) mixed with variable amounts of mEH (0−100 nM). The initial BP concentration was 10 μM, and the incubation time was 15 min at 37 °C. Reactions were quenched by the addition of ethyl acetate. The concentration of 3-OH (0.5 μM) is out of scale, but remained constant in all tested conditions. Left panel: experimental traces; right panel, simulated traces. Simulation was performed using the same equations and constants used in Figures 4 and 5.

(c) Influence of mEH to 1A1 Molar Ratio on BP Metabolite Profiles. Formation of phenols, dihydrodiols, and T2-tetrol was analyzed by mixing a fixed amount of 1A1-containing microsomes with a variable amount of mEH-containing microsomes and a complementary amount of control microsomes. Figure 6, left panel, shows that mEH addition caused an expected increase in the accumulation of 9,10-diol, concomitant with a decrease in 9-OH accumulation. Experimental half-saturation for T2-tetrol and 7,8-diol accumulations occurred for a similar value of the mEH to 1A1 ratio, thus indicating that the formation of T2-tetrol was mainly dependent upon 7,8-diol and not upon 9,10-diol concentration.

Correct simulation was performed with the same set of constants as used previously (Figure 6, left panel and right panel were superimposable). In addition, the simulation indicated that competition between enzymatic and nonenzymatic hydrolysis of the three BP-oxides was mainly related to their relative stabilities. Indeed, adjusted constants for 4,5-ox (k_{16} = 0.004 min^{-1}), 7,8-ox (k_{20} = 0.018 min^{-1}), and 9,10-ox (k_{17} = 0.1 min^{-1}) nonenzymatic hydrolysis were significantly different, which is consistent with half-life values found in the literature (*18*). By contrast, similar catalytic constants for 7,8-ox and 9,10-ox mEH-dependent hydrolysis led to correct simulation. V_{max} for 4,5-ox hydrolysis by mEH was chosen 2-fold higher than for 7,8-ox and 9,10-ox in order to fit experimental data. These results are in agreement with data obtained with the purified human enzyme (*20*).

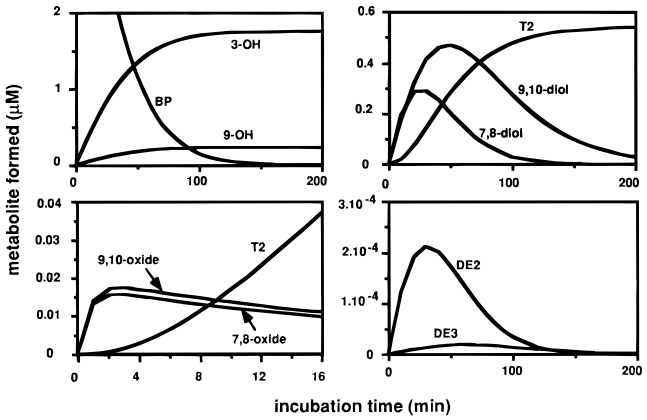

Figure 7. Simulated kinetics of the full metabolism of a single 10 μM BP dose by 5.8 nM 1A1 and 100 nM mEH. Simulation was performed as previously described using the rate constants listed in Table 3, with the exception that the inactivation constant k_1 was set at zero.

Model Based Predictions. Use of a unique model to simulate a wide range of experimental conditions (*i.e.*, time, substrate, 1A1 and mEH concentration dependencies) led to drastic constraints on certain kinetic parameters that would be only poorly defined based on a single experimental condition. We thus estimated that the kinetic model was valid and could be used to predict the time course for unstable species which are not experimentally measurable. This is particularly interesting in the case of genotoxic intermediates such as oxides and diol epoxides. To illustrate this potential, the time course for the complete metabolism of a single BP dose was predicted (Figure 7).

Based on numerical simulations, 9,10- and 7,8-ox accumulated very rapidly to reach a plateau after 2 min, while the level of 4,5-ox remained very low. Oxide concentrations were found to be at least 10-fold under the K_m of mEH, provided that the molar ratio between mEH and 1A1 was higher than 3, as expected in human liver (*21, 22*). In contrast, competitive inhibition between oxides was predicted to take place for lower mEH to 1A1 ratios, a likely situation occurring in human extrahepatic tissues (*22, 23*). DE2, the major genotoxic species, accumulated more slowly than BP-oxides to reach a maximum after about a half-hour and decayed during the 2 h which followed. Although diol epoxide hydrolysis was clearly a rapid process, its absolute rate was poorly determined by experimental data. Consequently, only the variation and the relative accumulations of DE2 and DE3 were significant. T2-tetrol formation was mainly driven by DE2 hydrolysis during the first hour. A contribution of 9,10-diol metabolism to T2-tetrol formation is predicted to be detectable after 2 h (about 20% of total T2-tetrol accumulation) due to the preferential accumulation of 9,10-diol following 1A1-dependent consumption of initially accumulated 7,8-diol. Simulations for various mEH amounts indicated that a mEH to 1A1 molar ratio as low as 0.01 was sufficient to account for about 10% of the maximal DE2 accumulation. Saturation of the mEH effect was observed for a mEH to 1A1 molar ratio of about 5. Although accumulation of T2-tetrol versus BP concentration (Figure 5) was bell-shaped when observed after a short incubation time (15 min), simulation of full BP conversion (5 h) following a single 10 μM dose indicated that total DE2 exposure was independent of the dose distribution (from 1 × 10 μM to 1000 times × 0.01 μM BP).

It should be observed that a potential limitation of the presented model is the absence of phase II-dependent conjugation reactions (with UDP-glucuronic acid and glutathione). These reactions are expected to reduce the level of BP-phenols, -dihydrodiols (*24*−*26*), and DE2 accumulation (*27, 28*). Nevertheless, since the presented model is based on microscopic rate constants, additional (particularly other phase II) reactions can be easily added without the requirement for novel adjustments of already determined kinetic parameters. Similarly, extension of the kinetic model to other P450 isoenzymes such as P450 2C8, 2C9, 2C18, and 3A4, which have been found to metabolize BP in our yeast expression system,[2] should also be attempted.

In conclusion, yeast-expressed human P450 1A1 and mEH were used to construct a minimal kinetic model of BP multistep metabolism which allowed the satisfactory reproduction, by numerical simulation, of the experimental kinetics of observable metabolites for all tested conditions. Such a validated model was then used to predict the genotoxic BP-oxide and -epoxide concentrations which cannot be quantified directly. Individual polymorphisms altering the expression level and enzymatic parameters have been documented in the case of BP-metabolizing enzymes such as glutathione *S*-transferase μ (*29*) and 1A1 (*30, 31*). It is anticipated that a complete model of BP metabolism would help to predict genotoxic risks associated with human polymorphisms, as interindividual changes in the expression level and an alteration of enzymatic parameters can be accounted for in numerical simulation.

Acknowledgment. This work was supported by Grants 6642 and 6604 from the Association pour la Recherche contre le Cancer and the Bioavenir program. We thank Dr. A. Seidel and Pr. F. Oesch for providing BP-tetrols and enantiomers of 7,8-diol. We also thank Dr. P. Dansette and S. Baird for helpful discussions.

References

(1) Kreyberg, L. (1954) The significance of histologic typing in the study of the epidemiology of primary epithelial lung tumors: a study of 466 cases. *Br. J. Cancer* **8**, 199−208.
(2) Wynder, E. L., and Graham, E. A. (1950) Tobacco smoking as a possible etiologic factor in bronchogenic carcinoma. *J. Am. Med. Assoc.* **143**, 329−336.
(3) Conney, A. H. (1982) Induction of microsomal enzymes by foreign chemicals and carcinogenesis by polycyclic aromatic hydrocarbons: G. H. A. Clowes Memorial Lecture. *Cancer Res.* **42**, 4875−4917.
(4) Roberts-Thomson, S. J., McManus, M. E., Tukey, R. H., Gonzalez, F. J., and Holder, G. M. (1993) The catalytic activity of four expressed human cytochrome P450s towards benzo[*a*]pyrene and the isomers of its proximate carcinogen. *Biochem. Biophys. Res. Commun.* **192**, 1373−1379.
(5) Shou, M., Korzekwa, K. R., Crespi, C. L., Gonzalez, F. J., and Gelboin, H. V. (1994) The role of 12 cDNA-expressed human, rodent and rabbit cytochromes P450 in the metabolism of benzo[*a*]pyrene and benzo[*a*]pyrene *trans*-7,8-dihydrodiol. *Mol. Carcinog.* **10**, 159−168.
(6) Bauer, E., Guo, Z., Ueng, Y.-F., Bell, C., Zeldin, D., and Guengerich, F. P. (1995) Oxidation of benzo[*a*]pyrene by recombinant human cytochrome P450 enzymes. *Chem. Res. Toxicol.* **8**, 136−142.
(7) Gautier, J.-C., Urban, P., Beaune, P., and Pompon, D. (1993) Engineered yeast cells as model to study coupling between human xenobiotic metabolizing enzymes. Simulation of the two first steps of benzo[*a*]pyrene activation. *Eur. J. Biochem.* **211**, 63−72.
(8) (1981) NIH guidelines for the laboratory use of chemical carcinogens. *NIH Publication* No. 81-2385, U.S. Government Printing Office, Washington, DC.

[2] Gautier, J.-C., Pfohl-Leszkowicz, A., Urban, P., Beaune, P., Pompon, D., manuscript in preparation.

(9) Urban, P., Cullin, C., and Pompon, D. (1990) Maximizing the expression of mammalian cytochrome P-450 monooxygenase activities in yeast cells. *Biochimie* **72**, 463−472.
(10) Cullin, C., and Pompon, D. (1988) Synthesis of functional mouse cytochromes P-450 P1 and chimeric P-450 P3−1 in the yeast *Saccharomyces cerevisiae*. *Gene* **65**, 203−217.
(11) Omura, T., and Sato, R. (1964) The carbon monoxide-binding pigment of liver microsomes. II-Solubilization, purification and properties. *J. Biol. Chem*. **239**, 2379−2387.
(12) Dahlquist, G., Björck, A., and Anderson, N. (1974) In *Numerical methods*, pp 346−347, Prentice-Hall, Englewood Cliffs, NJ.
(13) Thakker, D. R., Yagi, H., Lu, A. Y. H., Levin, W., Conney, A. H., and Jerina, D. M. (1976) Metabolism of benzo[*a*]pyrene: conversion of (±)-*trans*-7,8-dihydroxy-7,8-dihydrobenzo[*a*]pyrene to highly mutagenic 7,8-diol-9,10-epoxides. *Proc. Natl. Acad. Sci. U.S.A.* **73**, 3381−3385.
(14) Holder, G., Yagi, H., Dansette, P., Jerina, D. M., Levin, W., Lu, A. Y. H., and Conney, A. H. (1974) Effect of inducers and epoxide hydrase on the metabolism of benzo[*a*]pyrene by liver microsomes and a reconstituted system: Analysis by high pressure liquid chromatography. *Proc. Natl. Acad. Sci. U.S.A.* **71**, 4356−4360.
(15) Waterfall, J. F., and Sims, P. (1972) Epoxy derivatives of aromatic polycyclic hydrocarbons. The preparation and metabolism of epoxides related to benzo[*a*]pyrene and to 7,8- and 9,10-dihydrobenzo[*a*]pyrene. *Biochem. J*. **128**, 265−277.
(16) Bentley, P., Oesch, F., and Tsugita, A. (1975) Properties and amino acid composition of pure epoxide hydrolase. *FEBS Lett*. **59**, 296−299.
(17) Levin, W., Buening, M. K., Wood, A. W., Chang, R. L., Kedzierski, B., Thakker, D. R., Boyd, D. R., Gadaginamath, G. S., Amstrong, R. N., Yagi, H., Karle, J. M., Slaga, T. J., Jerina, D. M., and Conney, A. H. (1980) An enantiomeric interaction in the metabolism and tumorigenicity of (+)- and (−)-benzo[*a*]pyrene 7,8-oxide. *J. Biol. Chem*. **255**, 9067−9074.
(18) Levin, W., Wood, A. W., Yagi, H., Dansette, P. M., Jerina, D. M., and Conney, A. H. (1976) Carcinogenicity of benzo[*a*]pyrene 4,5-, 7,8-, and 9,10-oxides on mouse skin. *Proc. Natl. Acad. Sci. U.S.A*. **73**, 243−247.
(19) Plant, A. L., Knapp, R. D., and Smith, L. C. (1987) Mechanism and rate of permeation of cells by polycyclic aromatic hydrocarbons. *J. Biol. Chem*. **262**, 2514−2519.
(20) Lu, A. Y. H., Thomas, P. E., Ryan, D., Jerina, D. M., and Levin, W. (1979) Purification of human liver microsomal epoxide hydrolase. Differences in properties of the human and rat enzymes. *J. Biol. Chem*. **254**, 5878−5881.
(21) Schweikl, H., Taylor, J. A., Kitareewan, S., Linko, P., Nagorney, D., and Goldstein, J. A. (1993) Expression of CYP1A1 and CYP1A2 genes in human liver. *Pharmacogenetics* **3**, 239−249.
(22) DeWaziers, I., Cugnenc, P. H., Yang, C. S., Leroux, J.-P., and Beaune, P. H. (1990) Cytochrome P450 isoenzymes, epoxide hydrolase and glutathione transferases in rat and human hepatic and extrahepatic tissues. *J. Pharmacol. Exp. Ther*. **253**, 387−394.
(23) McLemore, T. L., Adelberg, S., Liu, M. C., McMahon, N. A., Yu, S. J., Hubbard, W. C., Czerwionski, M., Wood, T. G., Storeng, R., Lubet, R. A., Eggleson, J. C., Boyd, M. R., and Hines, R. N. (1990) Expression of human CYP1A1 gene in patient with lung cancer: evidence of cigarette smoke-induced gene expression in normal lung tissue and for altered gene regulation in primary pulmonary carcinomas. *J. Natl. Cancer Inst*. **82**, 1333−1339.
(24) Bock, K. W., Gschaidmeier, H., Seidel, A., Baird, S., and Burchell, B. (1992) Mono- and diglucuronide formation from chrysene and benzo[*a*]pyrene phenols by 3-methylcholanthrene-inducible phenols UDP-glucuronosyltransferase (UGT1A1). *Mol. Pharmacol*. **42**, 613−618.
(25) Hu, Z., and Wells, P. G. (1992) In vitro and in vivo biotransformation and covalent binding of benzo[*a*]pyrene in Gunn and RHA rats with a genetic deficiency in bilirubin uridine diphosphate-glucuronosyltransferase. *J. Pharmacol. Exp. Ther*. **263**, 334−342.
(26) Morgenstern, R., Guthenberg, C., Mannnervik, B., DePierre, J. W., and Ernster, L. (1982) Benzo[*a*]pyrene metabolism by rat liver microsomes: effects of adding purified glutathione S-transferases A, B and C. *Cancer Res*. **42**, 4215−4221.
(27) Ho, D., and Fahl, W. E. (1984) Modification of glutathione levels in C3H/10T1/2 cells and its relationship to benzo[*a*]pyrene *anti*-7,8-dihydrodiol 9,10-epoxide-induced cytotoxicity. *J. Biol. Chem*. **259**, 11231−11235.
(28) Jernström, B., Dock, L., Hall, M., Mannervik, B., Tahir, M. K., and Grover, P. L. (1989) Glutathione transferase catalyzed conjugaison of benzo[*a*]pyrene 7,8-diol 9,10-epoxide with glutathione in human skin. *Chem.-Biol. Interact*. **70**, 173−180.
(29) Hayashi, S., Watanabe, J., and Kawajiri, K. (1992) High susceptibility to lung cancer analyzed in terms of combined genotypes of P450 1A1 and Mu-class glutathione S-transferase genes. *Jpn. J. Cancer Res*. **83**, 866−870.
(30) Nebert, D. W., Petersen, D. D., and Puga, A. (1991) Human AH locus polymorphism and cancer: inducibility of CYP1A1 and other genes by combustion products and dioxin. *Pharmacogenetics* **1**, 68−78.
(31) Drakoulis, N., Cascorbi, I., Brockmöller, J., Gross, C. R., and Roots, I. (1994) Polymorphisms in the human CYP1A1 gene as susceptibility factors for lung cancer: exon-7 mutation (4889 A to G), and a T to C mutation in the 3′-flanking region. *Clin. Invest*. **72**, 240−248.

TX9500944